ROBUST OPTICAL PICOMETROLOGY THROUGH DATA DIVERSITY: SUPPLEMENTAL DOCUMENT

Superoscillatory wavefront synthesis

The computer-controlled wavefront synthesizer employed in this work is described in detail in Ref. [1]. It is based upon a pair of reflective liquid crystal spatial light modulators (Meadowlark P512) – one for intensity and the other for phase modulation, as shown schematically in Fig. S1.

In this work, we employ an axially-symmetric superoscillatory wavefront constructed from two circular prolate spheroidal wavefunctions, *S3* and *S4* (following Ref. [2]): $E(r/\lambda) = 4.477\, S3(r/\lambda) + S4(r/\lambda)$, where r is radial distance from the beam axis.

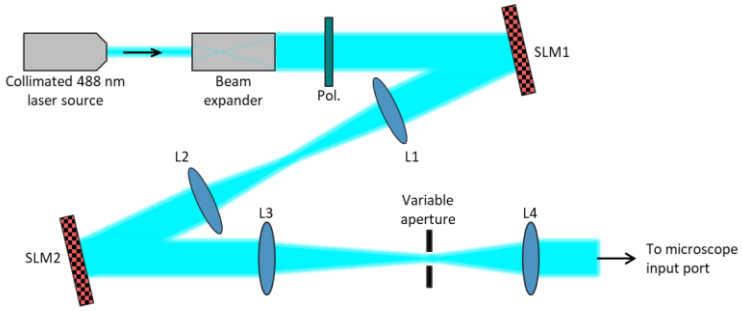

Fig. S1. Double-4*f* arrangement of spatial light modulators for superoscillatory wavefront synthesis: SLM = spatial light modulator; L = lens, Pol. = linear polarizer.

Neural network architecture and training

The neural network architecture is as reported in Ref. [3]. It is implemented using TensorFlow libraries and consists of three convolution layers, each followed by a pooling layer, with kernel dimensions as shown in Table S1. The network ends with three fully connected layers and a single output for nanowire displacement. Mean square error serves as the loss function, optimized with the Adam stochastic algorithm with a learning rate set at 0.0001. Training ends when the validation loss ceases to improve, monitored by setting an early stopping 'patience' of 400 epochs.

Table S1. Convolution neural network architecture

Layer Name	No. of Kernels	Kernel Size	Activation Function
Convolution 1	64	5 × 5	ReLu
Max Pooling 1	-	4 × 4	-
Convolution 2	128	4 × 4	ReLu
Max Pooling 2	-	3 × 3	-
Convolution 3	256	2 × 2	ReLu
Max Pooling 3	-	3 × 3	-
Fully Connected 1	128	-	ReLu
Fully Connected 2	256	-	ReLu
Fully Connected 3	128	-	ReLu
Output	1	-	Sigmoid

We recorded 19 consecutive sets of single-shot scattering patterns for 201 different nanowire positions, covering a displacement range of 360 - 4000 pm from the zero-bias position. The final set was designated as the 'measurement dataset', and never used in neural network training, except to establish precision and accuracy benchmarks for self-referenced training and testing within a single dataset. Others are designated as 'training datasets', as illustrated in Fig. 2. Among all sets, the same randomly selected 80% of scattering patterns and corresponding (known) nanowire displacement values were designated for use in neural network training and validation.

For each set of measurements (each of Figs. 3a-c, 4a-c, and equivalents for other values of Δt and N) the requisite $N \times 0.8 \times 201$ scattering patterns and nanowire displacement values (where N is the training depth – the number of 'training datasets' being used) were amalgamated in a single pool for training and validation. Across ten independent network implementations for each case, this pool is split in a randomized (i.e. differently for each implementation) 4:1 ratio between training ($N \times 128$ patterns) and validation ($N \times 32$ patterns).

For the purposes of Figs. 3, 4, and S2, every trained network is tested on the same set of ($0.2 \times 201 = 41$) scattering patterns for previously-unseen nanowire positions from the measurement dataset. For the purpose of Fig. 5, networks are also separately tested on scattering patterns from the measurement dataset for nanowire positions previously seen in training and validation.

Measurement performance at Δt = 10 min.

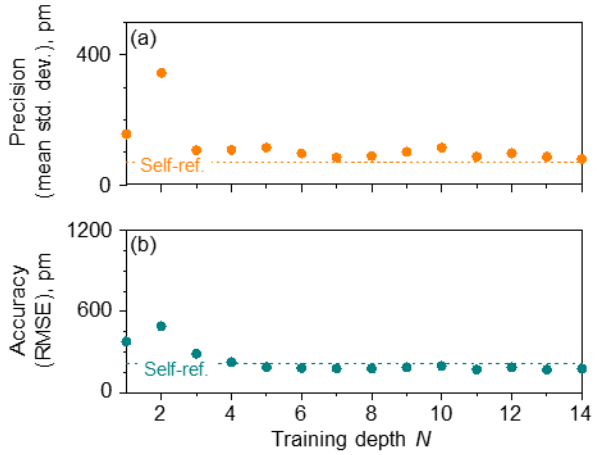

Fig. S2. Optical localization of nanowire position – performance as a function of training depth at Δt = 10 min. [Compare with Fig. 4d,e, showing performance at Δt = 5 min] (a) Measurement precision [average standard deviation] and (b) accuracy [root mean square error] as a function of training depth N.

References

[1] E. T. F. Rogers, S. Quraishe, K. S. Rogers, T. A. Newman, P. J. S. Smith, and N. I. Zheludev, "Far-field unlabeled super-resolution imaging with superoscillatory illumination," APL Photon. **5**, 066107 (2020).

[2] K. S. Rogers, K. N. Bourdakos, G. H. Yuan, S. Mahajan, and E. T. F. Rogers, "Optimising superoscillatory spots for far-field super-resolution imaging," Opt. Express **26**, 8095-8112 (2018).

[3] T. Liu, J. Y. Ou, J. Xu, E. A. Chan, K. F. MacDonald, and N. I. Zheludev, "Picophotonic localization metrology beyond thermal fluctuations," Nat. Mater. **22**, 844-847 (2023).